Atmos. Chem. Phys. Discuss., 2, 2449–2487, 2002
www.atmos-chem-phys.org/acpd/2/2449/

Atmospheric
Chemistry
and Physics
Discussions

# A novel model to predict the physical state of atmospheric $H_2SO_4/NH_3/H_2O$ aerosol particles

**C. A. Colberg, B. P. Luo, H. Wernli, T. Koop, and Th. Peter**

Institute for Atmospheric and Climate Science, Swiss Federal Institute of Technology, Zürich, Switzerland

Received: 14 November 2002 – Accepted: 21 November 2002 – Published: 16 December 2002

Correspondence to: C. A. Colberg (christina.colberg@ethz.ch)

## Abstract

The physical state of tropospheric aerosol particles is largely unknown despite its importance for cloud formation and for the aerosols' radiative properties. Here we show the first systematic global modelling study of the physical state of the $H_2SO_4/NH_3/H_2O$ aerosol, which constitutes an important class of aerosols in the free troposphere. The Aerosol Physical State Model (APSM) developed here is based on Lagrangian trajectories computed from ECMWF (European Centre for Medium Range Weather Forecasts) analyses, taking full account of the deliquescence/efflorescence hysteresis. As input APSM requires three data sets: (i) deliquescence and efflorescence relative humidities from laboratory measurements, (ii) ammonia-to-sulfate ratios (ASR) calculated by a global circulation model, and (iii) relative humidities determined from the ECMWF analyses. APSM results indicate that globally averaged a significant fraction (17–57%) of the ammoniated sulfate aerosol particles contain solids with the ratio of solid-containing to purely liquid particles increasing with altitude (between 2 and 10 km). In our calculations the most abundant solid is letovicite, $(NH_4)_3H(SO_4)_2$, while there is only little ammonium sulfate, $(NH_4)_2SO_4$. Since ammonium bisulfate, $NH_4HSO_4$, does not nucleate homogeneously, it can only form via heterogeneous crystallization. As the ammonia-to-sulfate ratios of the atmospheric aerosol usually do not correspond to the stoichiometries of known crystalline substances, all solids are expected to occur in mixed-phase aerosol particles. This work highlights the global importance of letovicite, whose role as cloud condensation nucleus (CCN) and as scatterer of solar radiation remains to be scrutinized.

## 1. Introduction

Aerosol particles in the atmosphere affect the radiative balance of the Earth through light scattering and absorption. Besides this direct climatic effect, aerosol particles contribute also indirectly as cloud precursors to the terrestrial radiation budget. Neither the direct nor the indirect effects are quantitatively well characterized, leading to large uncertainties in the global mean radiative forcing caused by aerosol particles, which may counteract the forcing by greenhouse gases to a large degree (IPCC, 2001).

The direct forcing by ”sulfate aerosols”, a commonly used abbreviation for partially ammoniated aqueous sulfuric acid particles, has been investigated in a number of studies (Charlson et al., 1991; Kiehl and Briegleb, 1993; Pilinis et al., 1995; Nemesure et al., 1995; Kiehl et al., 2000; Adams et al., 2001). The presence of sulfate in aerosol particles covers the range between sulfuric acid $H_2SO_4$ and ammonium sulfate $(NH_4)_2SO_4$ with intermediate compounds depending on the availability of gaseous ammonia to neutralize the sulfuric acid originating from the oxidation of sulfur dioxide (IPCC, 2001).

As these particles enhance the Earth’s albedo, their direct effect results in a net cooling. However, the level of confidence in the quantification of this effect is low (IPCC, 2001) due to the variety of sizes, shapes and refractive indices of sulfate aerosol particles. Their radiative forcing depends sensitively on the relative humidity (RH), because particle growth due to water uptake, and hence light scattering, is not linear in RH (Pilinis et al., 1995; Nemesure et al., 1995). The water content further depends on the degree of neutralization of the sulfate particles by ammonia (Adams et al., 1999). More importantly, partial neutralization by $NH_3$ makes the droplets amenable to partial crystallization, producing solid ammonium sulfate $(NH_4)_2SO_4$, ammonium bisulfate $NH_4HSO_4$, or letovicite $(NH_4)_3H(SO_4)_2$, with ammonium-to-sulfate-ratios ASR = 2.0, 1.5, and 1.0, respectively. Provided RH drops sufficiently low, the crystalline forms are thermodynamically favored (Clegg et al., 1998) and droplets may effloresce, depending on the ASR and temperature.

The optical properties of aerosol particles can change remarkably upon crystallization (Tang and Munkelwitz, 1991, 1994). However, as the stoichiometry of the droplets is unlikely to correspond precisely to ASR = 2.0, 1.5 and 1.0, the particles will develop mixed solid/liquid or mixed solid/solid phases, and radiative forcing estimations become even more complex.

In order to estimate the occurrence of solid-containing phases in the

$H_2SO_4/NH_3/H_2O$ aerosol system it is insufficient to know the ambient RH and the ASR at a given point in time, but the time history of the investigated air parcel needs to be known in order to account for the deliquescence/efflorescence hysteresis effect. For example, aqueous ammonium sulfate is saturated with respect to its crystalline phase at 82.6% RH at 260 K (Clegg et al., 1998; Onasch et al., 1999; Cziczo and Abbatt, 1999), whereas laboratory studies show that homogeneous crystallization of droplets does not occur before RH drops to about 32.7% (Onasch et al., 1999). Conversely, solid ammonium sulfate does not deliquesce at RH lower than 82.6%. Therefore, in the range $32.7\% < \mathrm{RH} < 82.6\%$ the physical state of such a particle in the atmosphere depends on its RH history which can be assessed only from Lagrangian air parcel trajectories.

In a general circulation model assessment of the sensitivity of direct climate forcing to hysteresis in anthropogenic sulfate aerosol particles Boucher and Anderson (1995) show that solid $(NH_4)_2SO_4$ particles have a 20% lower global cooling effect than if they remained liquid. Radiative transfer Julian day 180, at 12 pm and at $0^\circ \times 0^\circ$ by Martin (2002, unpublished results) indicate, depending on the Earth's underlaying reflectivity, differences in forcings of +3.81 to −0.91 $\mathrm{Wm}^{-2}$ when the aerosol is crystalline rather than aqueous in an atmospheric column at 80% RH.

The physical state of aerosol particles is also important for their ability to act as cloud condensation nuclei (CCNs) and has been discussed in the context of cirrus cloud formation (Martin, 1998; Bertram et al., 2000; Zuberi et al., 2001). Although the ice nucleation process largely determines the microphysical properties of cirrus clouds and therefore their climate forcing potential (DeMott et al., 2001), the exact role of aerosol particles in cirrus formation remains unclear (Martin, 2000). This also illustrates the need for a detailed microphysical investigation of the physical state of atmospheric aerosol particles.

Ammonia and sulfate are known for a long time to be components of the atmospheric aerosol particles, and their importance is also corroborated by recent studies (Li et al., 1997; Talbot et al., 1998; Dibb et al., 1999; Liu et al., 2000; Chow et al., 1999). Of course, tropospheric aerosol particles are not only a mixture of $H_2SO_4/NH_3/H_2O$, but may also contain nitrate, sea salt, organic compounds and elemental carbon. Their composition varies widely with geographical location and altitude (Seinfeld and Pandis, 1998). Recent time of flight mass spectrometry measurements of single atmospheric aerosol particles by Noble and Prather (1996), Murphy et al. (1998) and Held et al. (2002) highlight the importance of organics and elemental carbon besides water soluble inorganic compounds. In this sense, the restriction of the present study to the subclass $H_2SO_4/NH_3/H_2O$ represents only a first step towards a comprehensive modelling of the physical state of tropospheric aerosol particles.

Despite the importance for the Earth's radiation balance, there is a lack in our understanding of the physical state of atmospheric aerosol particles, and also in particular of the $H_2SO_4/NH_3/H_2O$ class investigated here. This lack in knowledge is due to the difficulty of field measurements having to determine the physical state of individual particles in the sub-micron range simultaneously with RH and ASR measurements (the latter from a single particle composition measurement). In the free troposphere such simultaneous measurements of single aerosol particles have not been performed to date. However, there are some field measurements of the physical state of boundary layer aerosol particles, which show that supersaturated particles exist, even at low RH (McMurry and Stolzenburg, 1989; Rood et al., 1989; Shaw and Rood, 1990; McMurry et al., 1996). In principle, atmospheric aerosol particles can remain liquid or crystallize homogeneously or heterogeneously depending on their chemical composition. At present, it is not clear which are the most important mechanisms (Martin, 2000).

The goal of this work is to apply state-of-the-art laboratory data on the homogeneous efflorescence and deliquescence of the $H_2SO_4/NH_3/H_2O$ aerosol system to the atmosphere in order to predict, for the first time, the physical state of this aerosol class globally. For this purpose we use trajectories derived from ECMWF analyses. As input parameters we use global RH-fields, also from the ECMWF analyses, and ASR data from a GCM-study by Adams et al. (1999). RH values are then tracked along trajectories.

## 2. Methodology

### 2.1. Input parameters

The process that dry solid crystals stay dry upon humidification but take up water spontaneously above a certain RH to form an aqueous solution is called deliquescence, and the corresponding RH value thermodynamically required for this to happen is called deliquescence relative humidity (DRH). The inverse process of solidification is called efflorescence and, in contrast to deliquescence, is not thermodynamically determined but is a kinetic phenomenon, which requires supersaturation. The RH value typically required for solidification is called efflorescence relative humidity (ERH). Because DRH > ERH, there is a deliquescence/efflorescence-hysteresis. In case DRH and ERH are known functions of temperature ($T$) and ASR, and provided that 3-dimensional atmospheric fields of ASR and RH values are available, the physical state of an aerosol of a given composition can be predicted from air parcel trajectory analysis.

For $H_2SO_4/NH_3/H_2O$ aerosol particles our Aerosol Physical State Model combines the 3-D time-dependent input fields ASR($x, y, z, t$), RH($x, y, z, t$) and $T(x, y, z, t)$, and tracks ERH($T$,ASR) and DRH($T$,ASR) time-dependently along trajectories.

### 2.1.1. Efflorescence and deliquescence relative humidities (ERH and DRH)

For DRH we use the thermodynamic model of the $H_2SO_4/NH_3/H_2O$ system by Clegg et al. (1998), which has been verified by a number of laboratory studies (Yao et al., 1999; Chelf and Martin, 1999; Koop et al., 1999; Cziczo and Abbatt, 1999; Onasch et al., 1999). For efflorescence we assume crystallization to occur via homogeneous nucleation in the APSM. This allows us to obtain a lower bound for the formation of solid-containing particles. Although heterogeneous nuclei occur quite frequently in the atmosphere (Martin, 2000) their influence on atmospheric nucleation processes is still uncertain.

The limited data available in the literature on low temperature ERH are restricted to the $(NH_4)_2SO_4/H_2O$ system (ASR = 2) (Cziczo and Abbatt, 1999; Onasch et al., 1999). Therefore, we performed nucleation experiments with single aerosol particles in an electrodynamic particle trap to obtain additional ERH values for ASR and $T$ of atmospheric relevance (Colberg, 2001; Colberg et al., 2003). The experimental setup is described in more detail elsewhere (Krieger et al., 2000; Colberg, 2001; Colberg et al., 2003). In brief, these experiments make use of the DC-voltage as direct measurement of the particle mass and therefore of concentration changes. In addition, the particle radii are calculated by Mie-phase-function-analysis (Davis and Periasamy, 1985). Information on the particle shape and morphology is further obtained with light-scattering intensity fluctuation measurements (Braun and Krieger, 2001; Krieger and Braun, 2001). Finally, Raman-spectra are taken in order to identify the investigated particles. The composition of the gas phase, pressure (100 mbar - 1000 mbar) and temperature (158 K - 310 K) are controlled in the chamber. Since particles can be kept in the trap for weeks, measurements can be performed on a long time scale. The measured ERH values which are used for this study are shown in Table 1.

Figure 1 shows ERH data of the $(NH_4)_2SO_4/H_2O$ (ASR = 2) system as a function of temperature and RH together with the saturation curves for ice (solid gray line) and $(NH_4)_2SO_4$ (solid red line) predicted by the model of Clegg et al. (1998). The dashed red line is calculated by subtracting a constant $\Delta$ RH from the DRH curve. This was motivated by the procedure of Koop et al. (2000) who suggested that homogeneous nucleation of ice from aqueous solutions would occur at a concentration differing by a constant RH (or water activity) from the melting point curve. Note that the constant $\Delta$ RH for $(NH_4)_2SO_4$ and for ice differ in sign. Here we subtract 50% RH from the DRH curve, call this curve the $\Delta$50-curve, and suggest that it corresponds to the ERH. The agreement between the measured data and the $\Delta$50-curve supports this procedure. The dashed gray line is the homogeneous nucleation ice curve, which Koop et al. (2000) obtained by adding a constant 30.5% RH to the ice melting point curve. As a result the red and gray shaded areas show the ranges where purely liquid aerosol particles cannot exist due to homogeneous nucleation of crystalline $(NH_4)_2SO_4$ or ice, respectively. The hysteresis phenomenon is illustrated by the blue/red water uptake or loss trajectories, which represent atmospherically possible pathways. A cooling (i.e. humidifying) process starting at dry conditions (D) leaves the particles solid until RH > DRH at the corresponding temperature (D') is reached. In the reverse warming (i.e. drying) process starting from (E) the aerosol will crystallize only when RH < ERH at the corresponding temperature (E') is reached (as long as heterogeneous nuclei are absent).

Figure 2 shows DRH and ERH at two different temperatures as a function of RH and ASR. The DRH curves are calculated using the model of Clegg et al. (1998). The left panel ($T$ = 260 K) shows averaged measurements by Colberg (2001) and Colberg et al. (2003) (solid triangles for nucleation at ASR = 1 and 1.5, and open circle for ASR = 0.5 indicating no nucleation) together with the value for ASR = 2 from from Fig. 1. The red line is calculated again by subtracting 50% RH from the DRH curve and is in good agreement with the measured data. The good agreement between the measurements and the Δ50-curve suggests, that the particle trap experiments at 260 K probably succeeded in measuring homogeneous nucleation, as we would expect a strong heterogeneous effect to result in considerable scatter. Thus, the Δ50-method represents a physically motivated approximation, which despite the lack of more closely spaced ERH measurements allows a reasonable approximation of the efflorescence behavior of atmospheric $H_2SO_4/NH_3/H_2O$ aerosol particles. In the lack of any information at lower temperatures we use the Δ50-method also at temperatures lower than $T$ = 260 K.

The red curve in the right panel for $T$ = 293 K was again calculated by subtracting 50% RH. Electrodynamic balance measurements by Tang and Munkelwitz (1994) are plotted as solid gray triangles, electrodynamic balance measurements by Spann and Richardson (1985) as solid black circles. The gray and black bars show the scatter of their data, illustrating that they definitely observed not only homogeneously but also heterogeneously triggered crystallization. Looking for an approximation for homogeneous efflorescence we could adopt the lower envelope of their data. However, when taking the absolute values of their scattering into account the Δ50-method (red curve) is again a suitable approach to obtain ERH input parameters for $T = 293$ K, as it satisfies the lower bound criterion and follows at the same time the physical picture given by Koop et al. (2000). Therefore we use the Δ50-method for 220 K, 260 K and 293 K and interpolate DRH and ERH at intermediate temperatures during a model run.

The crystallization we observe for ASR = 1 and $T = 260$ K is in contradiction to measurements by Cziczo and Abbatt (2000), who did not obverse crystallization for temperatures between 298 and 238 K in a flow tube study. This might be due to residence times in the flow reactor of approximately 30 s, which might be too short to allow nucleation and crystallization to be observed. In contrast to these observations we propose that letovicite indeed forms through homogeneous nucleation at ERH = 16% ± 2.5%, since we identified it during 18 independent efflorescence cycles as the crystallization product. We do this based on the fact that we have obviously no problem in avoiding heterogeneous nucleation in our electrodynamic particle trap, as both $(NH_4)_2SO_4$ and NaCl nucleate exactly at the accepted homogeneous ERH values (Colberg, 2001; Braun and Krieger, 2001; Krieger and Braun, 2001; Colberg et al., 2003), reported in the literature (Martin, 2000).

### 2.1.2. Ammonia to sulfate ratios (ASR)

Adams et al. (1999) developed a global circulation model (GCM) for tropospheric sulfate, nitrate and ammonia aerosol particles which provides ASR. From this we derive ASR climatologies for January and July. They use GEIA (Global Emission Inventory Activity) emission data, compare and match their results with available measured ASR. Adams et al. (1999) report that their modeled values are generally within a factor of two to the existing data. The GCM provides ASR with a $4^\circ \times 5^\circ$ horizontal resolution at 959, 849, 786, 634, 468, 321 and 201 mbar. For the use in the APSM we binned the ASR values in the altitude ranges 0–200, 200–400, 400–600, 600–800 and 800–1000 mbar. As an example, Fig. 3 shows the global ASR averaged for the month of July in the 400–600 mbar bin (around 5 km altitude). The figure shows ASR close to complete neutralization at northern middle and high latitudes resulting from the high ammonia emissions from microbiological soil activity and livestock farming during the summer months in the northern hemisphere, but very low particulate ammonium in the higher latitude southern hemisphere.

### 2.1.3. Trajectories

The APSM allows to accurately model the deliquescence/efflorescence hysteresis by tracking the temporal development of ASR and RH along air parcel trajectories. Three-dimensional, month-long trajectories are started at the beginning of the two months of July 2000 and January 2001 on four levels 700, 600, 500 and 400 mbar, using ECMWF wind fields from the T319L60 assimilation cycle. This is done on a 5° × 5° grid from 180° W to 180° E and from 85 ° S to 85° N. This results in 4 × 72 × 35 = 10080 trajectories for each time period. A closer description of the trajectory tool is given by Wernli and Davies (1997). Every six hours RH and temperature are interpolated to the trajectory positions (latitude, longitude and altitude).

## 2.2. Model description

Along with the 5 altitude bins (0–200, 200–400, 400–600, 600–800 and 800–1000 mbar) the 5° × 5° intervals yield a total of 12960 model grid boxes. The 10080 trajectories are initialized and after a three-day adjustment period the aerosol investigation is started.

In each grid box the physical state of the aerosols is analyzed for all intersecting trajectories at each 6-hr time step: The aerosol on a trajectory entering a grid box whose (RH,ASR)-pair is below the corresponding ERH crystallizes, forming mixed-phase (solid/liquid) particles. Upon further transport the solid components survive as long as the trajectory does not enter a grid box whose (RH,ASR)-pair is above the corresponding DRH, in which case the particles will again become fully liquid. Figure 4 shows the temporal evolution of RH on a typical trajectory (solid and dash-dotted gray line). The blue and red lines show the corresponding DRH and ERH, which depend on the time depend ASR and $T$ along the trajectory. Therefore the solid gray line represents periods with mixed phase particles whereas the dash-dotted gray line shows periods with purely liquid aerosol particles. On the basis of this procedure the physical state of the $H_2SO_4/NH_3/H_2O$ aerosol particles is identified along all 10080 trajectories, from which the fraction of particles containing solid ammonium sulfate [$(NH_4)_2SO_4$], letovicite [$H_2SO_4/NH_3/H_2O$], or ammonium bisulfate [$NH_4HSO_4$] relative to the total number of all $H_2SO_4/NH_3/H_2O$ aerosol particles can be determined in each grid box. From this also area-weighted global mean values are calculated.

## 3. Results and discussion

The results of the APSM are discussed in detail for the altitude range 400-600 mbar for the month of July. Results for other altitudes and for January are shown subsequently. The 400-600 mbar bin corresponds to the free troposphere around 5 km, an altitude where $H_2SO_4/NH_3/H_2O$ particles have also been observed over maritime regions (Yamato and Tanaka, 1994; Talbot et al., 1998; Dibb et al., 1999). A reliable analysis of this altitude range was enabled by ERH measurements (Colberg, 2001; Colberg et al., 2003), which were performed at $T = 260$ K, a typical temperature at these altitudes. Figure 5 shows the fraction of solid-containing $H_2SO_4/NH_3/H_2O$ particles. Red colors correspond to areas of a solid-containing fraction of at least 50%. There are large regions with high fractions of solid-containing aerosol particles, particularly above continents. During the northern hemispheric summer the occurrence of partially solidified $H_2SO_4/NH_3/H_2O$ particles is pronounced because both the natural as well as the anthropogenic mean ammonia emissions are high (Bouwman et al., 1997). In contrast to ammonia emissions, the precursor emissions of sulfate vary geographically and seasonally to a lower extent (Adams et al., 1999).

The main advantage of this trajectory study is that the deliquescence/efflorescence hysteresis is modeled accurately. Depending on the history of the air parcel, the aerosol particles might be liquid despite being supersaturated. Figure 6 shows the result if the hysteresis phenomenon is not considered and crystallization is assumed to happen without supersaturation. Clearly, such a purely thermodynamic treatment, which neglects kinetic barriers suppressing efflorescence, massively overestimates the fraction of solid-containing particles.

The benefit of a trajectory study is further highlighted by the result presented in Figure 7. Here, as in Fig. 6 the kinetics of efflorescence are not taken into account, but in addition Lagrangian information along trajectories is neglected as the calculation is performed in a purely Eulerian, grid-based approach: Each grid-box was checked for RH and taken as containing solids for RH $<$ DRH and as liquid for RH $>$ DRH (as function of ASR and $T$). This results in a purely thermodynamic snap-shot, similar to what could be achieved by a three-dimensional model, which does not allow to quantify a fraction which contains solids, rather the particles are either liquid (blue areas) or solid (red areas).

### 3.1. Partitioning between letovicite and ammonium sulfate

As long as we assume crystallization to occur exclusively via homogeneous nucleation, only letovicite and ammonium sulfate may form in the APSM. The bisulfate cannot form homogeneously, as is evident from the efflorescence curves in Fig. 2 and discussed in detail in Sect. 3.5.1 (see also Fig. 11). It could only nucleate heterogeneously, for example on preexisting letovicite or ammonium sulfate, a case which is discussed as a sensitivity study in detail in Sect. 3.5.1, where also details of the homogeneous pathways are given. Here we restrict ourselves to homogeneous crystallization of letovicite and ammonium sulfate, and consider their partitioning.

Figure 8 shows the global distribution of letovicite (left panel) and ammonium sulfate fractions (right panel). The fraction of ammonium sulfate is very low, and almost all mixed-phase particles contain letovicite. This study demonstrates that letovicite is the prominent solid phase of the $H_2SO_4/NH_3/H_2O$ system.

### 3.2. Altitudinal dependence

The altitudinal dependence of the fraction of solid-containing $H_2SO_4/NH_3/H_2O$ particles is illustrated in Fig. 9 for the 200–400, 400–600 and 600–800 mbar bins in July. Results for the 0–200 and 800–1000 mbar bins are not displayed due to too large uncertainties of the input parameters in these areas. The fraction of solid-containing particles increases with altitude due to the decrease in RH and $T$ (affecting ERH). In particular, the solid material in the upper troposphere (200–400 mbar) of the southern hemisphere is due to low temperatures in this region, illustrating the importance of measurements of ERH at low $T$.

### 3.3. Seasonal variation

For January the fraction of solid-containing $H_2SO_4/NH_3/H_2O$ particles is illustrated in Fig. 10 for the 400-600 mbar level. Though the global fraction of mixed-phase $H_2SO_4/NH_3/H_2O$ particles is clearly smaller in January than in July due to reduced microbiological activity, still a significant amount of solid-containing aerosol particles is to be expected. The seasonal fluctuation of the ASR is influenced strongly by the variations in ammonia emissions while sulfate emissions remain relatively uniform (Adams et al., 1999). The larger amounts of solid-containing aerosol particles in the southern hemisphere are due to increased oceanic ammonia production in the southern hemispheric summer.

### 3.4. Global mean values

The global monthly mean values of RH, ASR, solid-containing aerosol fraction and the partitioning of ammonium sulfate and letovicite for July and January are listed in Tables 2 and 3. In order to enable global mean value calculations the results have been weighted by the surface areas of each grid box.

### 3.5. Sensitivity studies

We have tested the importance of errors introduced by the various input parameters (DRH, ERH, ASR and RH) along trajectories. In general we find a variation of about 5% in any one of these input parameter sets to be hardly visible in the resulting geographical plots of solid-containing fractions. The resulting global mean values of the total solid-containing fraction differed by less than 2%. The overall result of significant amounts of mixed-phase ammoniated sulfate particles, and particularly of letovicite remains unaffected.

#### 3.5.1. Immediate heterogeneous nucleation of a second solid

Up to now we have assumed homogeneous crystallization to be the only process leading to solid-containing aerosol particles. However a second approach, namely to assume that an immediate heterogeneous nucleation of a second solid takes place after homogeneous nucleation occurred, has to be considered.

These two approaches and the resulting microphysical consequences are explained by means of Fig. 11. Two possible microphysical pathways – (i) and (ii) – as well as the thermodynamically stable phases in the $H_2SO_4/NH_3/H_2O$ system are illustrated. The saturation curves ($S = 1$) for ammonium bisulfate (solid red line), letovicite (solid blue line) and ammonium sulfate (solid green line) are shown as a function of RH and ASR. In a drying process $H_2SO_4/NH_3/H_2O$ aerosol particles are supersaturated with respect to solid phases once these saturation curves are intersected (i.e. points (I) and 1) in Fig. 11). In the homogeneous nucleation only scenario, letovicite or ammonium sulfate can nucleate only below the corresponding homogeneous efflorescence lines (intersections (II) and (2) with the dashed blue and green line, respectively). Ammonium bisulfate cannot form at all, since its theoretical homogeneous ERH-value is lower than 0%. Subsequent to crystallization, when the air humidifies again and/or when the aerosol acidifies (due to uptake of additional $H_2SO_4$), the solids deliquesce fully once the corresponding saturation curve is intersected, which means that the RH > DRH (i.e.

intersections (III) and (3)). Recrystallization cannot occur before RH falls below ERH again. This assumption has been used for the APSM calculations shown in Figs. 5, 8, 9 and 10.

As an alternative to the homogeneous nucleation only scenario, homogeneous nucleation could immediately be followed by heterogeneous nucleation of a second solid. This means that homogeneous nucleation initiates heterogeneous nucleation. This allows the possibility of ammonium bisulfate formation. Therefore more phases and a higher percentage of solid-containing particles are expected when compared to the mere homogeneous case. Besides the two mixed phases ammonium sulfate/liquid and letovicite/liquid the mixed phase ammonium bisulfate/liquid as well as the two mixed solid phases letovicite/ammonium sulfate and ammonium bisulfate/letovicite can be formed. This is illustrated by the two microphysical pathway (i) and (ii) in Fig. 11. Instead of deliquescing at the saturation curve of the solid that was formed initially (intersections (III) and (3)), the particles do not fully deliquesce before the corresponding saturation curve of any one component of the mixed phase is intersected (i.e. intersections (IV) and (4)). For the scenario that homogeneous nucleation initiates heterogeneous nucleation, the total fraction of solid-containing aerosol particles and the partitioning of the three occurring solids ammonium bisulfate, letovicite and ammonium sulfate are illustrated in Fig. 12. The global monthly mean values for July and the corresponding partitioning of the solid phases are listed in Table 4.

The global mean values of the total solid-containing fraction are enhanced by 6% at maximum. A significant difference between the two scenarios is that the partitioning shifts once heterogeneous nucleation is considered. Ammonium bisulfate is obtained in quite substantial amounts. Although the total letovicite fraction is reduced because of ammonium bisulfate formation, letovicite is still a dominant solid phase in the $H_2SO_4/NH_3/H_2O$ system. The ammonium sulfate fraction remains unaffected.

It would be rather speculative to assess which of the two examined cases is the more realistic one, since the role of heterogeneous salt crystallization in the atmosphere is uncertain. However the case of homogeneous crystallization can be regarded as a lower bound for the formation of solid-containing particles (compare Figs. 5, 8, 9 and 10.

### 3.5.2. Treatment of RH close to ice saturation

One problem can result from the special treatment of RH in ECMWF analyses. ECMWF assumes ice particles to form immediately, to sediment out and to readjust RH to ice saturation at the moment that ice saturation (solid gray line in Fig. 1) is reached. In contrast, laboratory aerosol particles can be massively supersaturated before ice nucleation occurs (Cziczo and Abbatt, 1999; Koop et al., 1999; Bertram et al., 2000; Koop et al., 2000; Martin, 2000). Since the ECMWF analyses do not allow supersaturation with respect to ice to occur, this treatment may affect our analysis as it disables the deliquescence of solid ammoniated sulfate particles at temperatures below the eutectic point of ice and the ammonium salts. To obtain a lower bound for the presence of solid-containing particles in the calculations described above we put RH to the value of the corresponding homogeneous ice nucleation point in the moment a trajectory intersects the ice saturation curve. This yields a lower limit for the presence of solid ammoniated sulfate particles since it allows deliquescence below the eutectic point. Since the above method provides a lower limit of solid-containing aerosol particles a sensitivity run was performed, in which exclusively ECMWF RH-values are used even if the ice saturation curve is intersected. In this run the global mean values of the total solid-containing aerosol fraction are barely higher: In the 200–400 mbar bin 5% more solid-containing particles are observed whereas in the other two bins the values differ by less than 1%. This is largely due to the fact that the trajectories infrequently reach ice saturation.

### 3.6. Summary

In an Eulerian, thermodynamic, grid-based approach the consideration of globally averaged RH- and ASR-values leads to a misleading estimate of the fraction of solid-containing aerosol particles when compared to our trajectory study. Results of the APSM show that over large areas more than 50% of all aerosol particles contain solid particles. The solid-containing fraction consists particularly of letovicite, which therefore has to be discussed with respect to its atmospheric relevance. These results are rather insensitive to season and altitude. Depending on the treatment of homogeneously induced heterogeneous crystallization in the model ammonium bisulfate can be formed as well.

In future, the model could be extended with regard to following topics:

Initial heterogeneous nucleation – Crystallization would occur at higher ERH-values, which means that the fraction of solid-containing aerosol particles would increase. For such a scenario global concentrations of heterogeneous nuclei like mineral dust or soot are needed.

Implementation of nitric acid – The GCM study of Adams et al. (1999) provides $HNO_3$-data. In order to implement $HNO_3$ into the APSM, laboratory ERH data are needed. However, there is only limited data on the quaternary system ($H_2SO_4/NH_3/HNO_3/H_2O$). Pure ammonium nitrate shows small crystallization tendency (Cziczo and Abbatt, 2000; Dougle et al., 1998). Kriescher et al. (2003) show that ammonium sulfate can nucleate from mixed ammonium sulfate/ammonium nitrate solutions. Although the global nitrate concentrations are much smaller than sulfate concentrations (Adams et al., 1999) the effect of additional $HNO_3$ needs to be investigated.

Implementation of organic compounds and soot particles - Apart from the fact that the exact composition of atmospheric aerosol particles is not known, no GCM data and only limited ERH- and DRH-values (Choi and Chan, 2001, 2002; Brooks et al., 2002) are available for a system including organic constituents. Therefore such an extension would be extremely difficult and is not possible at this point.

## 4. Conclusions

The treatment of the $H_2SO_4/NH_3/H_2O$ system is a first step towards global aerosol physical state modelling, which allows an estimation of the occurrence of solid-containing particles in the atmosphere. The direct aerosol forcing effect is very sensitive to the water uptake properties of the particles (Adams et al., 2001). Therefore the physical state of atmospheric aerosol particles is of high importance. Since we can predict the physical state of atmospheric aerosol particles with our APSM these information can now be used in direct aerosol forcing calculations.

The results of this study show that mixed-phase ammoniated sulfate particles, mainly containing letovicite, are expected to occur frequently on a global scale. This is in agreement to Tabazadeh and Toon (1998), who are the only authors discussing the atmospheric relevance of letovicite. Hence, the atmospheric relevance of letovicite needs to be investigated with respect to its chemical and radiative properties. In contrast, current models which calculate the radiative forcing of atmospheric aerosol particles take sulfate aerosol particles either as fully ammoniated (i.e. ammonium sulfate) or as pure sulfuric acid (Adams et al., 2001).

Based on the present study we recommend that the optical properties (size, shape and refractive index) of letovicite and the morphology of mixed-phase particles containing letovicite and a remaining liquid should be studied in order to understand the influence of these mixtures on the radiative balance.

*Acknowledgements.* We are very grateful to P. J. Adams for providing data sets of ammonia-to-sulfate ratios. We thank U. K. Krieger for his support in accomplishing the laboratory experiments and for many helpful discussions. Thanks also to Y. Kriescher for providing some additional experimental data. C. A. Colberg is grateful to D. Brunner for an introduction into HIPHOP. We thank S. T. Martin for providing unpublished results. We acknowledge internal funding by the Swiss Federal Institute of Technology (ETH).

## References

Adams, P. J., Seinfeld, J. H., and Koch, D. M.: Global concentrations of tropospheric sulfate, nitrate, and ammonium aerosol simulated in a general circulation model, Journal of Geophysical Research, 104, 13 791–13 823, 1999. 2451, 2453, 2457, 2459, 2461, 2465, 2478

Adams, P. J., Seinfeld, J. H., Koch, D. M., Mickley, L., and Jacob, D.: General circulation model assessment of direct radiative forcing by the sulfate-nitrate-ammonium-water inorganic aerosol system, Journal of Geophysical Research, 106, 1097–1111, 2001. 2451, 2466

Bertram, A. K., Koop, T., Molina, L. T., and Molina, M. J.: Ice formation in $(NH_4)_2SO_4$-$H_2O$ particles, Journal of Physical Chemistry A, 104, 584–588, 2000. 2452, 2464

Boucher, O. and Anderson, T. L.: General circulation model assessment of the sensitivity of direct climate forcing by anthropogenic sulfate aerosols to aerosol size and chemistry, Journal of Geophysical Research, 100, 26 117–26 134, 1995. 2452

Bouwman, A. F., Lee, D. S., Asman, W. A. H., Dentener, F. J., VanderHoek, K. W., and Olivier, J. G. J.: A global high-resolution emission inventory for ammonia, Global Biogeochemical Cycles, 14, 561–587, 1997. 2459

Braun, C. and Krieger, U. K.: Two dimensional angular light scattering in aqueous NaCl single aerosol particles during deliquescence and efflorescence, Optics Express, 8, 314–321, 2001. 2455, 2457

Brooks, S. D., Wise, M. E., Cushing, M., and Tolbert, M. A., Deliquescence behavior of organic/ammonium sulfate aerosol, Geophysical Research Letters, 29, 1917, doi:10.1029/2002GL014733, 2002. 2465

Charlson, R. J., Langner, J., Rhode, H., Leovy, C. B., and Warren, S. G.: Perturbation of the Northern-Hemisphere radiative balance by backscattering from anthropogenic sulfate aerosols, Tellus, 43, 152–163, 1991. 2451

Chelf, J. and Martin, S.: Water activity and equilibrium freezing temperatures of aqueous $NH_4HSO_4$ solutions from −30 to 25° C, Journal of Geophysical Research, 26, 2391–2394, 1999. 2454

Choi, M. Y. and Chan, C. K.: Continuous measurements of the water activities of aqueous droplets of water-soluble organic compounds, Journal of Physical Chemistry A, 106, 4566–4572, 2001. 2465

Choi, M. Y. and Chan, C. K.: The effects of organic species on the hygroscopic behaviors of inorganic aerosols, Environmental Science and Technology, 36, 2422–2428, 2002. 2465

Chow, J. C., Watson, J. G., Edgerton, S. A., and Vega, E.: Chemical composition of PM2.5 and PM10 in Mexico City during winter 1997, Science of the Total Environment, 26, 2391–2394, 1999. 2452

Clegg, S. L., Brimblecombe, P., and Wexler, A. S.: A thermodynamic model of the system $H^+$-$NH_4^+$-$SO_4^{2-}$-$NO_3^-$-$H_2O$ at tropospheric temperatures, Journal of Physical Chemistry A, 102, 2137–2154, http://www.hpc1.uea.ac.uk/~e770/aim.html, 1998. 2451, 2452, 2454, 2455, 2456, 2476, 2477

Colberg, C. A.: Experiment an levitierten $H_2SO_4/NH_3/H_2O$-Aerosolteilchen: Atmosphärische Relevanz von Letovizit, Dissertation 14331, ETH Zürich, 2001. 2455, 2456, 2457, 2459, 2472, 2476, 2477

Colberg, C. A., Krieger, U. K., and Peter, T.: Morphological investigations during deliquescence- and efflorescence-cycles of $H_2SO_4/NH_3/H_2O$ aerosol particles, in preparation, 2003. 2455, 2456, 2457, 2459, 2472, 2476, 2477

Cziczo, D. J. and Abbatt, J. P. D.: Deliquescence, efflorescence, and supercooling of ammonium sulfate aerosols at low temperature: Implications for cirrus cloud formation and aerosol phase in the atmosphere, Journal of Geophysical Research, 104, 13 781–13 790, 1999. 2452, 2454, 2455, 2464, 2476

Cziczo, D. J. and Abbatt, J. P. D.: Infrared observations of the response of NaCl, MgCl2, NH4HSO4, and NH4NO3 aerosols to changes in relative humidity from 298 to 238 K, Journal of Physical Chemistry A, 104, 2038–2047, 2000. 2457, 2465

Davis, E. J. and Periasamy, R.: Light scattering and aerodynamic size measurements for homogeneous and inhomogeneous microspheres, Langmuir, 1, 373–379, 1985. 2455

DeMott, P., Lynch, D. K., Sassen, K., and Starr, D.: Cirrus, Oxford University Press, London, 2001. 2452

Dibb, J. E., Talbot, R. W., Scheuer, E. M., Blake, D. R., Blake, N. J., Gregory, G. L., Sachse, G. W., and Thornton, D. C.: Aerosol chemical composition and distribution during the Pacific Exploratory Mission (PEM) tropics, Journal of Geophysical Research, 104, 5785–5800, 1999. 2452, 2459

Dougle, P. J., Veefkind, J. P., and ten Brink, H. M.: Crystallisation of mixtures of ammonium nitrate, ammonium sulphate and soot, Journal of the Atmospheric Sciences, 29, 375–386, 1998. 2465

Held, A., Hinz, K. P., Trimborn, A., Spengler, B., and Klemm, O.: Chemical classes of atmospheric aerosol particles at a rural site in Central Europe during winter, Journal of the Atmospheric Sciences, 33, 581–594, 2002. 2453

IPCC: Intergovernmental Panel on Climate Change: Third Assessment Report: Climate Change 2001, The Scientific Basis, Summary for Policymakers, WMO/UNEP, Cambridge University Press, 2001. 2451

Kiehl, J. T. and Briegleb, B. P.: The relative roles of sulfate aerosols and greenhouse gases in climate forcing, Science, 260, 311–314, 1993. 2451

Kiehl, J. T., Schneider, T. L., Rasch, P. J., and Barth, M. C.: Radiative forcing due to sulfate aerosols from simulations with the National Center for Atmospheric Research Community Climate Model - Version 3, Journal of Geophysical Research, 105, 1441–1457, 2000. 2451

Koop, T., Bertram, A. K., Molina, L. T., and Molina, M. J., Phase transitions in aqueous $NH_4HSO_4$ solutions, Journal of Physical Chemistry A, 103, 9042–9048, 1999. 2454, 2464

Koop, T., Luo, B. P., Tsias, A., and Peter, T.: Water activity as the determinant for homogeneous ice nucleation in aqueous solutions, Nature, 406, 611–614, 2000. 2455, 2457, 2464, 2476

Krieger, U. K. and Braun, C.: Light-scattering intensity fluctuations in single aerosol particles, Journal of Quantitative Spectroscopy and Radiative Transfer, 70, 545–554, 2001. 2455, 2457

Krieger, U. K., Colberg, C. A., Weers, U., Koop, T., and Peter, T.: Supercooling of single $H_2SO_4/H_2O$ aerosols to 158 K: No evidence for the occurrence of the octahydrate, Geophysical Research Letters, 27, 2097–2100, 2000. 2455

Kriescher, Y., Krieger, U. K., and Peter, T.: Efflorescence behavior of single levitated ammonium sulfate/ammonium nitrate-aerosol particles at low temperatures, in preparation, 2003. 2465

Li, S. M., Macdonald, A. M., Strapp, J. W., and Lee, Y. N.: Chemical and physical characterizations of atmospheric aerosols over southern California, Journal of Geophysical Research, 102, 21 341–21 353, 1997. 2452

Liu, D. Y., Prather, K. A., and Hering, S. V.: Variations in the size and chemical composition of nitrate-containing particles in riverside, CA, Aerosol Science and Technology, 33, 71–86, 2000. 2452

Martin, S. T.: Phase transformations of the ternary system $(NH_4)_2SO_4$-$H_2SO_4$-$H_2O$ and the implications for cirrus cloud formation, Geophysical Research Letters, 25, 1657–1660, 1998. 2452

Martin, S. T.: Phase transitions of aqueous atmospheric particles, Chemical Reviews, 100, 3403–3453, 2000. 2452, 2453, 2454, 2457, 2464

McMurry, P. H. and Stolzenburg, M. R.: On the sensitivity of particle-size to relative-humidity for los angeles aerosols, Atmospheric Environment, 23, 497–507, 1989. 2453

McMurry, P. H., Litchy, M., Huang, P. F., Cai, X. P., Turpin, B. J., Dick, W. D., and Hanson, A.: Elemental composition and morphology of individual particles separated by size and hygroscopicity with the TDMA, Atmospheric Environment, 30, 101–108, 1996. 2453

Murphy, D. M., Thomson, D. S., and Mahoney, T. M. J.: In situ measurements of organics, meteoritic material, mercury, and other elements in aerosols at 5 to 19 km, Science, 282, 1664–1669, 1998. 2453

Nemesure, S., Wagener, R., and Schwartz, S. E.: Direct shortwave forcing of climate by the anthropogenic sulfate aerosol: Sensitivity to particle size, composition, and relative humidity, Journal of Geophysical Research, 100, 26 105–26 116, 1995. 2451

Noble, C. A. and Prather, K. A.: Real-time measurement of correlated size and composition profiles of individual atmospheric aerosol particles, Environmental Science and Technology, 30, 2667–2680, 1996. 2453

Onasch, T. B., Siefert, R. L., Brooks, S. D., Prenni, A., Murray, B., Wilson, M., and Tolbert, M. A.: Infrared spectroscopic study of the deliquescence and efflorescence of ammonium sulfate aerosol as a function of temperature, Journal of Geophysical Research, 104, 21 317–21 326, 1999. 2452, 2454, 2455, 2476

Pilinis, C., Pandis, S. N., and Seinfeld, J. H.: Sensitivity of direct climate forcing by atmospheric aerosols to aerosol-size and composition, Journal of Geophysical Research, 100, 18 739–18 754, 1995. 2451

Rood, M. J., Shaw, M. J., Larson, T. V., and Covert, D.: Ubiquitous nature of ambient metastable aerosol, Nature, 337, 537–539, 1989. 2453

Seinfeld, J. H. and Pandis, S. N.: Atmospheric chemistry and physics, John Wiley and Sons Inc., New York, 1998. 2453

Shaw, M. A. and Rood, M. J., Measurement of the crystallization humidities of ambient aerosol-particles, Atmospheric Environment, 24, 1837–1841, 1990. 2453

Spann, J. F. and Richardson, C. B.: Measurement of the water cycle in mixed ammonium acid sulfate particles, Atmospheric Environment, 19, 819–825, 1985. 2456, 2477

Tabazadeh, A. and Toon, O. B.: The role of ammoniated aerosols in cirrus cloud nucleation, Geophysical Research Letters, 25, 1379–1382, 1998. 2466

Talbot, R. W., Dibb, J. E., and Loomis, M. B.: Influence of vertical transport on free tropospheric aerosols over the central USA in springtime, Geophysical Research Letters, 25, 1367–1370,

1998. 2452, 2459

Tang, I. N. and Munkelwitz, H. R.: Simultaneous determination of refractive index and density of an evaporating aqueous solution droplet, Aerosol Science and Technology, 15, 201–207, 1991. 2451

Tang, I. N. and Munkelwitz, H. R., Water activities, densities, and refractive indices of aqueous sulfates and sodium nitrate droplets of atmospheric importance, Journal of Geophysical Research, 99, 801–808, 1994. 2451, 2456, 2477

Wernli, H. and Davies, H. C.: A Lagrangian-based analysis of extratropical cyclones. (1) The method and some applications, Quarterly Journal Of The Royal Meteorological Society, 123, 467–489, 1997. 2458

Yamato, M. and Tanaka, H.: Aircraft observations of aerosols in the free marine troposphere over the North Pacific Ocean: Particle chemistry in relation to air mass origin, Journal of Geophysical Research, 99, 5353–5377, 1994. 2459

Yao, Y., Massucci, M., Clegg, S. L., and Brimblecombe, P., Equilibrium water partial pressures and salt solubilities in aqueous $NH_4HSO_3$ to low temperatures, Journal of Physical Chemistry A, 103, 3678–3686, 1999. 2454

Zuberi, B., Bertram, A. K., Koop, T., Molina, L. T., and Molina, M. J.: Heterogeneous freezing of aqueous particles induced by crystallized $(NH_4)_2SO_4$, ice, and letovicite, Journal of Physical Chemistry A, 105, 6458–6464, 2001.

2452

**Table 1.** ERH-values from nucleation experiments of single, levitated aerosol particles in an electrodynamic particle trap (Colberg, 2001; Colberg et al., 2003). ERH-values are averages from 1-4 experiments. Measurements are performed at constant temperatures, the errors are ± 2.5% in RH

| ASR | ERH / % homogeneous | $T$ / K | solid phase |
|---|---|---|---|
| 2 | 30.8 | 263.5 | $(NH_4)_2SO_4$ |
| 2 | 28.5 | 260.0 | $(NH_4)_2SO_4$ |
| 1.5 | 27.5 | 263.5 | $(NH_4)_3H(SO_4)_2$ |
| 1 | 16.0 | 270.0 | $(NH_4)_3H(SO_4)_2$ |
| 1 | 16.0 | 264.0 | $(NH_4)_3H(SO_4)_2$ |
| 1 | 15.0 | 260.0 | $(NH_4)_3H(SO_4)_2$ |
| 0.5 | < 1.0 | 263.5 | no nucleation |
| 0.3 | < 1.0 | 263.5 | no nucleation |
| 0 | < 1.0 | 258–290 | no nucleation |

**Table 2.** Global monthly mean values for July calculated from the results of the APSM

| Altitude / mbar | RH / % | ASR | Fraction / % total solid | Fraction / % $(NH_4)_3H(SO_4)_2$ | Fraction / % $(NH_4)_2SO_4$ |
|---|---|---|---|---|---|
| 200–400 | 40.3 | 1.1 | 56.9 | 54.5 | 2.4 |
| 400–600 | 41.5 | 1.0 | 33.9 | 28.8 | 4.2 |
| 600–800 | 50.4 | 1.0 | 19.7 | 14.6 | 5.1 |

**Table 3.** Global monthly mean values for January calculated from the results of the APSM

| Altitude / mbar | RH / % | ASR | Fraction / % total solid | Fraction / % $(NH_4)_3H(SO_4)_2$ | Fraction / % $(NH_4)_2SO_4$ |
|---|---|---|---|---|---|
| 200–400 | 42.7 | 0.8 | 38.3 | 38.0 | 0.3 |
| 400–600 | 42.1 | 0.8 | 23.6 | 23.3 | 0.3 |
| 600–800 | 48.9 | 0.8 | 17.4 | 16.7 | 0.7 |

**Table 4.** Global monthly mean values for July calculated from the results of the APSM for the sensitivity study: Homogeneous nucleation initiates heterogeneous nucleation

| Altitude / mbar | RH / % | ASR | Fraction / % total solid | Fraction / % $NH_4HSO_4$ | Fraction / % $(NH_4)_3H(SO_4)_2$ | Fraction / % $(NH_4)_2SO_4$ |
|---|---|---|---|---|---|---|
| 200–400 | 40.3 | 1.1 | 57.0 | 29.7 | 24.5 | 2.9 |
| 400–600 | 41.5 | 1.0 | 38.8 | 16.2 | 18.4 | 4.2 |
| 600–800 | 50.4 | 1.0 | 24.0 | 7.1 | 12.8 | 4 |

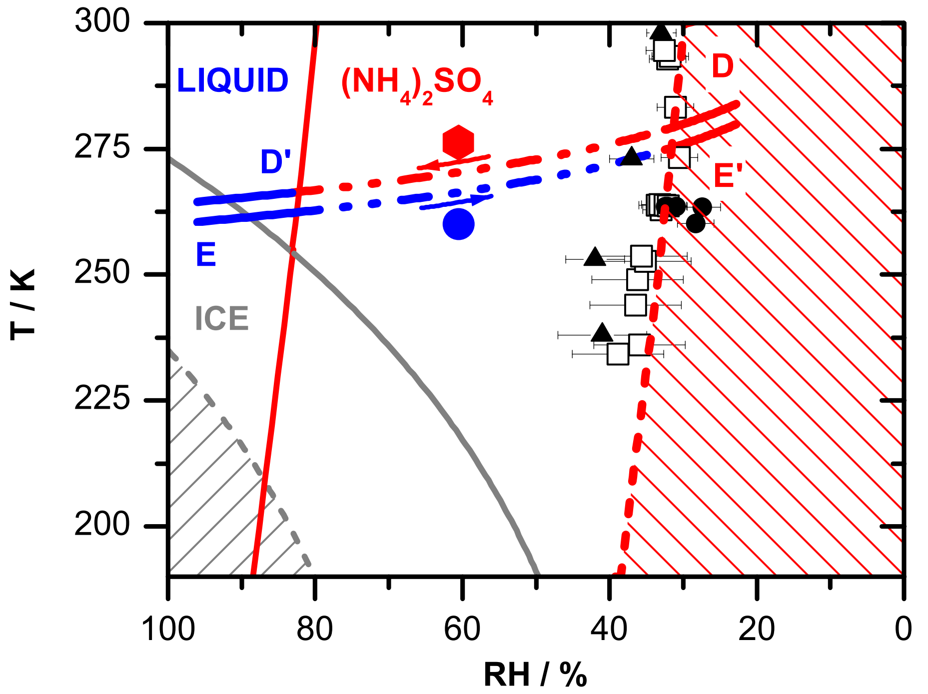

**Fig. 1.** Phase diagram of the $(NH_4)_2SO_4/H_2O$-system (ASR = 2). Temperature and RH ranges are shown together with the saturation curves for ice (solid grey line) and $(NH_4)_2SO_4$ (solid red line) predicted by the model of Clegg et al. (1998). The solid circles (measurements in an electrodynamic balance by Colberg (2001); Colberg et al. (2003)), the open squares (flow tube studies by Onasch et al. (1999)) and the solid triangles (flow tube studies by Cziczo and Abbatt (1999)) show efflorescence measurements with the corresponding error bars. The dashed red line is calculated by subtracting 50 % RH from the DRH curve and is called the Δ50-curve. It represents the homogeneous nucleation line of $(NH_4)_2SO_4$. The dashed grey line is the homogeneous ice nucleation curve (Koop et al., 2000). The hysteresis phenomenon is illustrated by the blue/red water uptake trajectories.

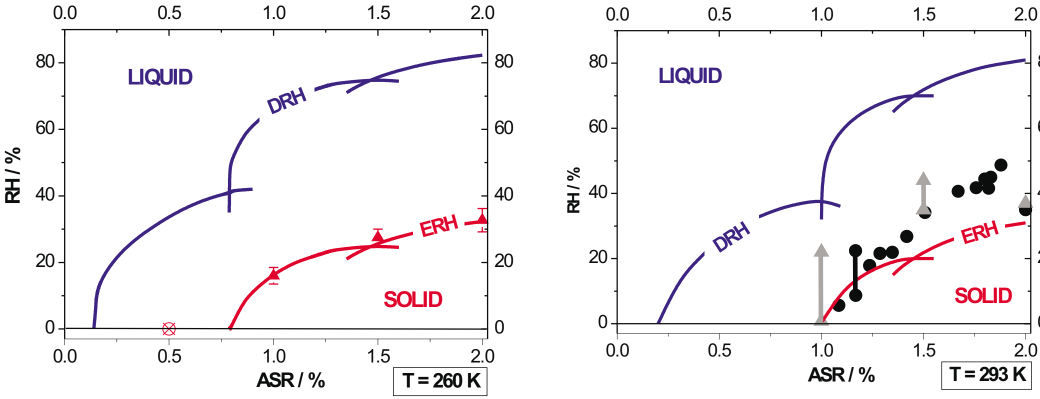

**Fig. 2.** DRH- and ERH-values at two different temperatures as a function of RH and ASR. The DRH curves are calculated by the model of Clegg et al. (1998). The left panel (T = 260 K) shows measurements by Colberg (2001); Colberg et al. (2003) (solid triangles for ASR = 1 and 1.5, the open circle for ASR = 0.5 indicates that no nucleation was observed) and the value which resulted for ASR = 2 from Fig. 1. The red line is calculated by subtracting 50 % RH from the DRH values and is called theΔ50-curve. The red line in the left panel was calculated likewise and is in very good agreement with the data. Measurements by Tang and Munkelwitz (1994) are plotted as solid grey triangles and measurements by Spann and Richardson (1985) are plotted as solid black circles. The grey and black bars show the scattering of their data.

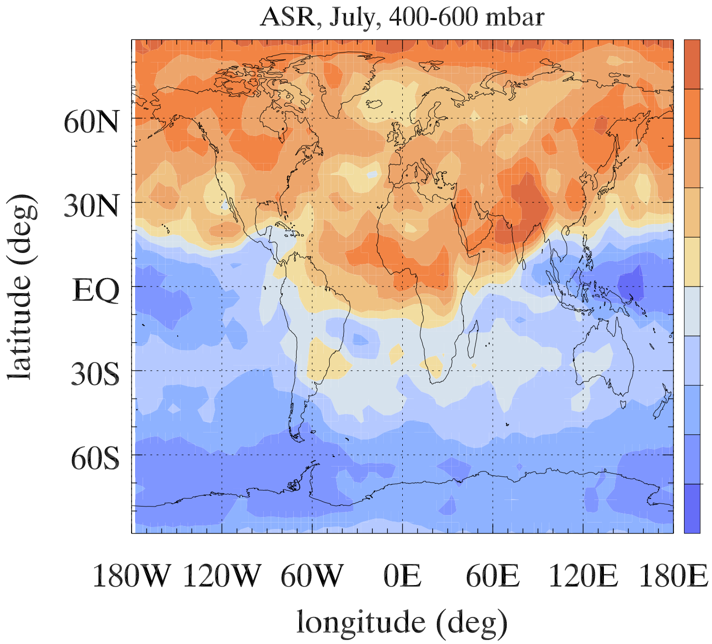

**Fig. 3.** Ammonia to sulfate ratios (ASR) from Adams et al. (1999) are used as an input parameter for the APSM. Global ASR values are illustrated and averaged for the month of July in the 400–600 mbar bin.

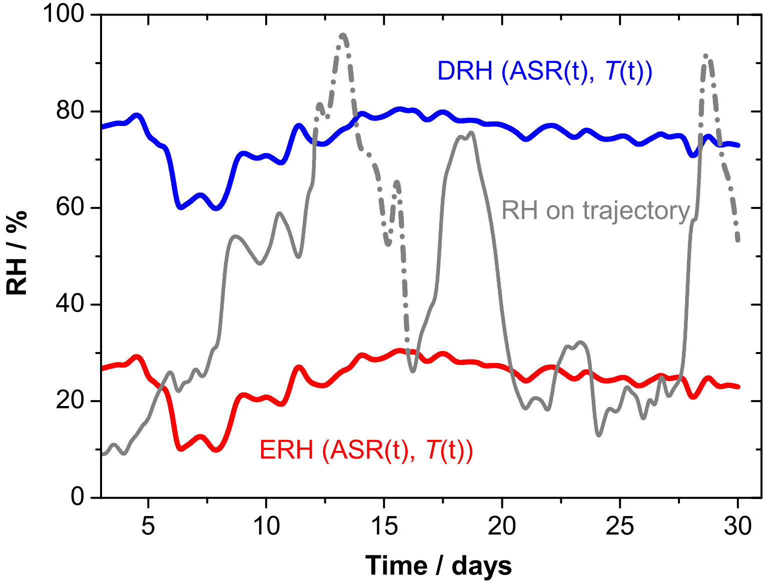

**Fig. 4.** The temporal RH-progression of a typical trajectory is displayed (solid and dashed grey line). The blue and red lines show the corresponding DRH and ERH. The solid grey line represents solid particles whereas the dashed grey line indicates totally liquid aerosol particles.

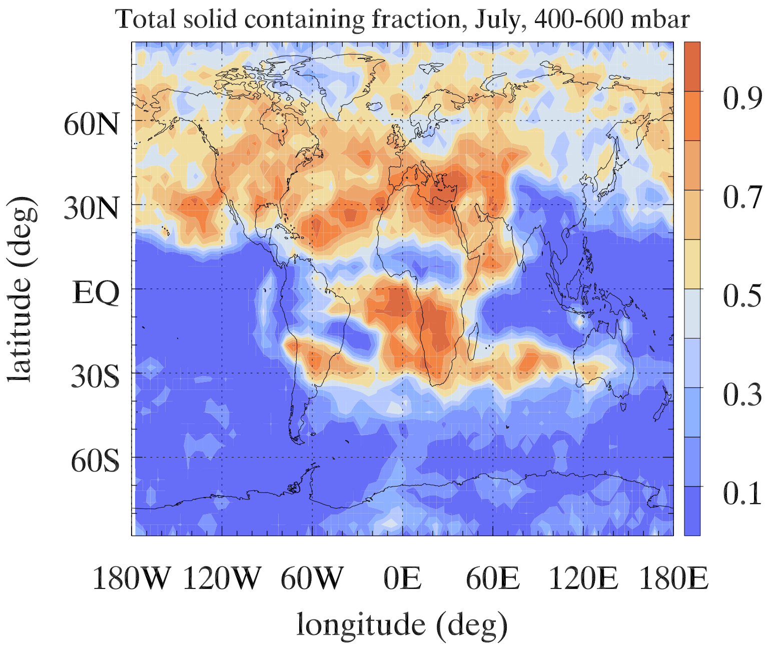

**Fig. 5.** Fraction of solid-containing $H_2SO_4/NH_3/H_2O$ particles in July for the 400–600 mbar bin. Results are obtained by a trajectory study.

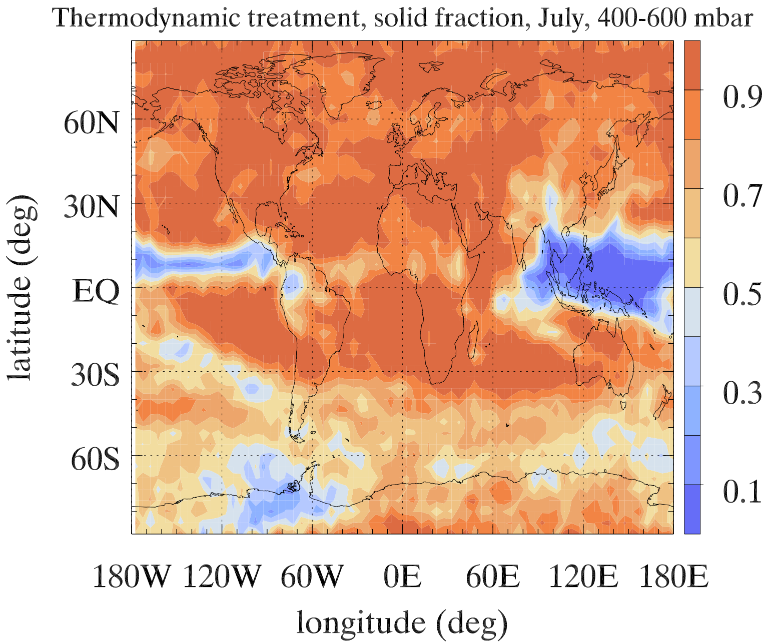

**Fig. 6.** Fraction of solid-containing $H_2SO_4/NH_3/H_2O$ particles in July for the 400–600 mbar bin. Results are obtained by a trajectory study but crystallization is assumed to occur without supersaturation.

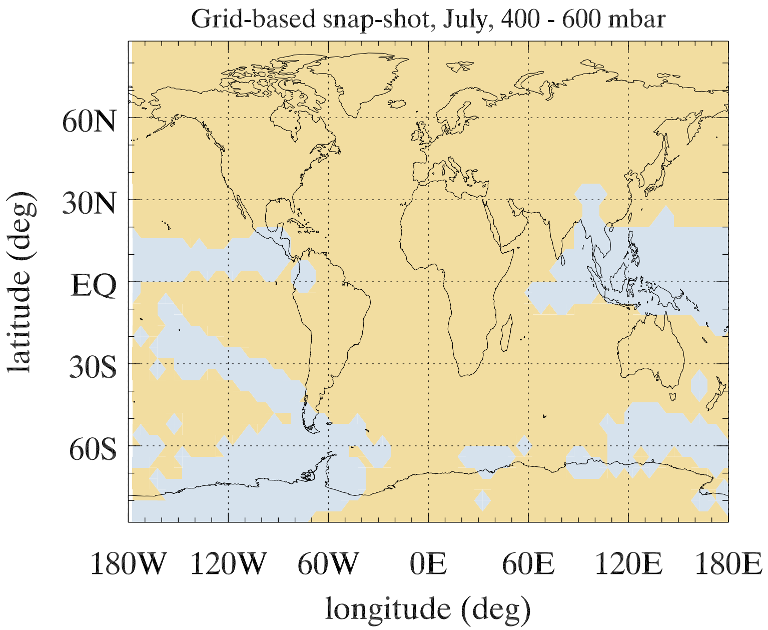

**Fig. 7.** Result of an Eulerian, grid-based approach. Purely thermodynamic snap-shot of a distribution of liquid (blue) and solid (red) $H_2SO_4/NH_3/H_2O$ particles (July, 400–600 mbar). The aerosol particles are taken as solid for RH < DRH and as liquid for RH > DRH.

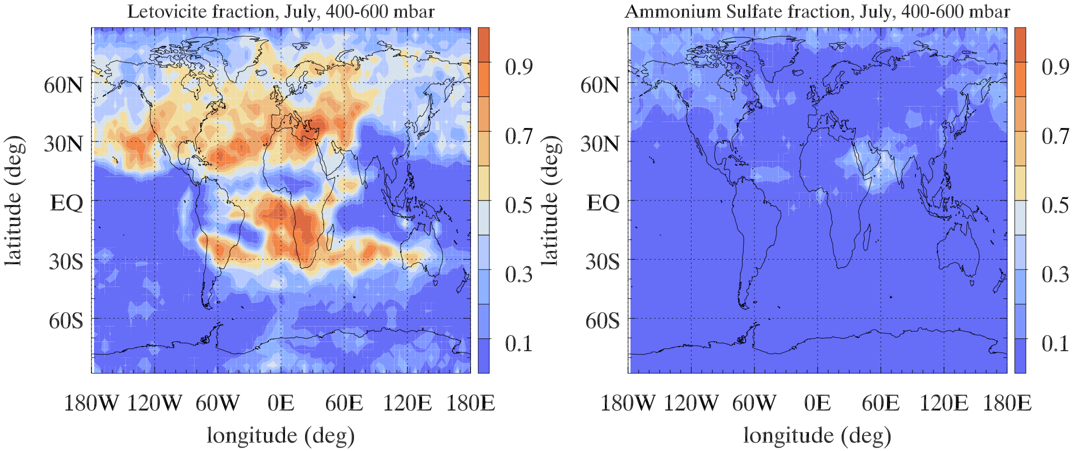

**Fig. 8.** Partitioning of the solid-containing fraction of $H_2SO_4/NH_3/H_2O$ particles in July for the 400–600 mbar bin. Global letovicite and ammonium sulfate fractions are shown for the homogeneous nucleation scenario.

Title Page
Abstract Introduction
Conclusions References
Tables Figures
◀◀ ▶▶
◀ ▶
Back Close
Full Screen / Esc
Print Version
Interactive Discussion

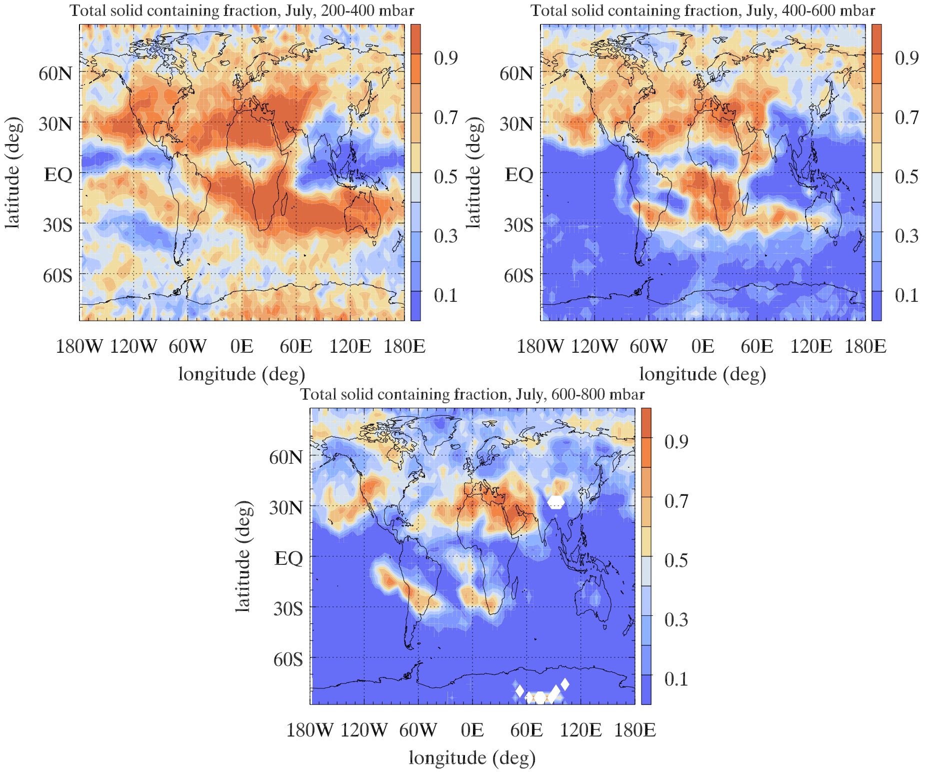

**Fig. 9.** Altitudinal comparison of the fraction of solid-containing $H_2SO_4/NH_3/H_2O$ particles in July for the 200–400, 400–600 and 600–800 mbar bins. White sectors characterize grid boxes which were not crossed by any trajectory.

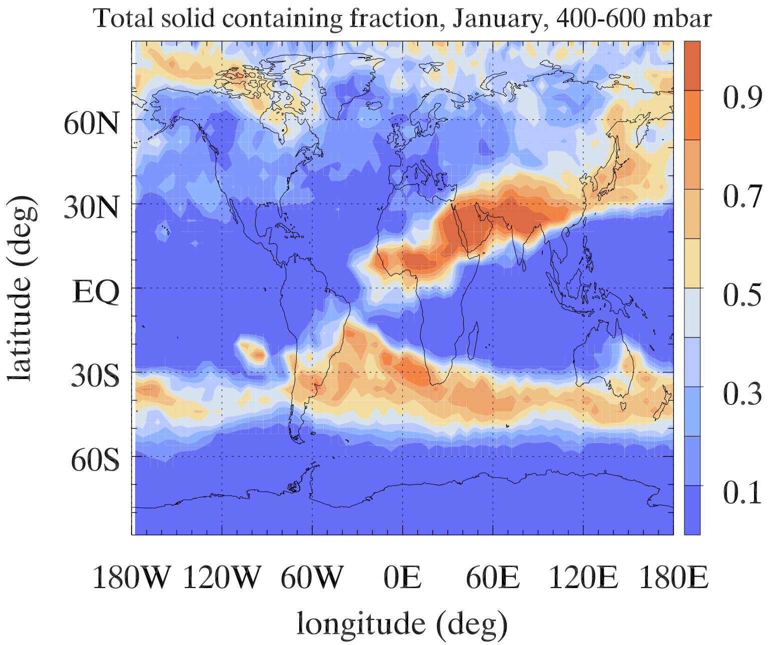

**Fig. 10.** Fraction of solid-containing $H_2SO_4/NH_3/H_2O$ particles in January for the 400–600 mbar bin.

Title Page
Abstract
Introduction
Conclusions
References
Tables
Figures
◄
►
◄
►
Back
Close
Full Screen / Esc
Print Version
Interactive Discussion

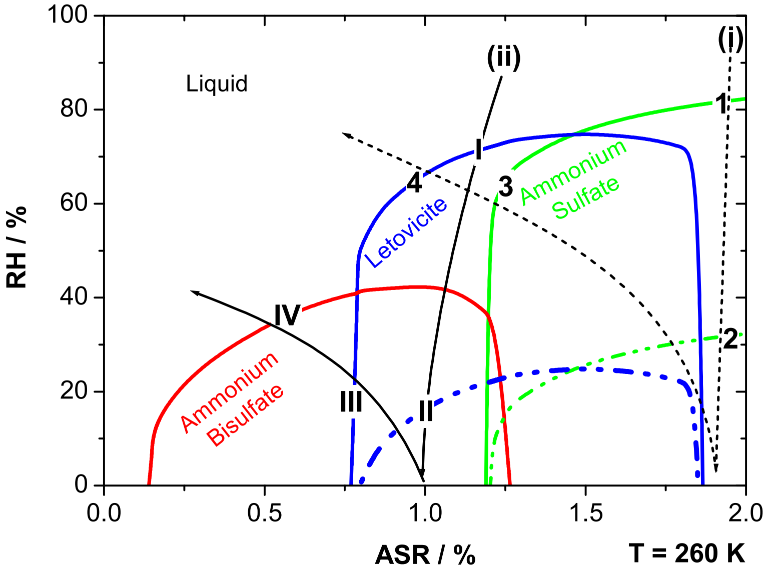

**Fig. 11.** Phase diagram of the $H_2SO_4/NH_3/H_2O$ system. The saturation curves for ammonium bisulfate (solid red line), letovicite (solid blue line) and ammonium sulfate (solid green line) are shown as a function of RH and ASR. The dashed blue and green lines correspond to homogeneous efflorescence lines of letovicite and ammonium sulfate, respectively, which are derived in Fig. 2. Moreover two possible microphysical pathways – indicated by the dotted black line (i) and the solid black line (ii) – are illustrated in order to explain the differences between the two approaches: (a) mere homogeneous nucleation and (b) immediate heterogeneous nucleation of a second solid after homogeneous nucleation.

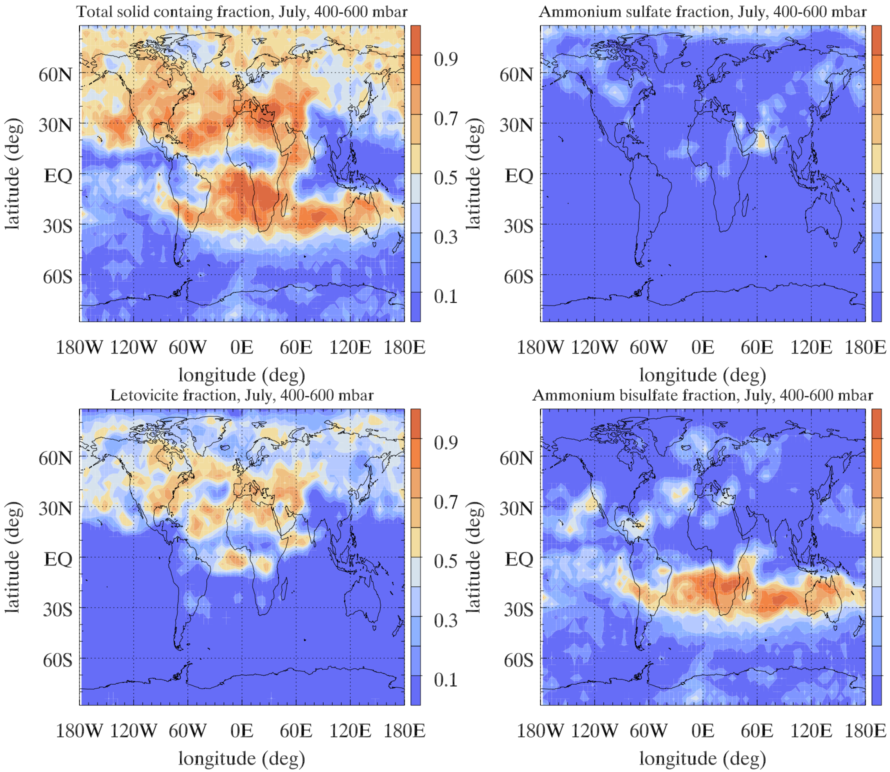

**Fig. 12.** Sensitivity study: Immediate heterogeneous nucleation of a second solid after homogeneous nucleation. Fraction of solid-containing $H_2SO_4/NH_3/H_2O$ particles and the partitioning of the three solids ammonium sulfate, letovicite and ammonium bisulfate in July for the 400–600 mbar bin.